Waalbot: An Agile Small-Scale Wall-Climbing Robot Utilizing Dry Elastomer Adhesives

Michael P. Murphy, *Student Member, IEEE*, and Metin Sitti, *Fellow, IEEE*

***Abstract*—This paper proposes a small-scale agile wall-climbing robot, which is able to climb on smooth vertical surfaces using flat adhesive elastomer materials for attachment. Using two actuated legs with rotary motion and two passive revolute joints at each foot, this robot can climb and steer in any orientation. Due to its compact design, a high degree of miniaturization is possible. It has onboard power, computing, and wireless communication, which allow for semiautonomous operation. Various aspects of a functioning prototype design and performance are discussed in detail, including leg and foot design and gait dynamics. A model for the adhesion requirements and performance is developed and verified through experiments. Using an adhesive elastomer (Vytaflex 10), the current prototype can climb 90° slopes at a speed of up to 6 cm/s and steer to any angle reliably on a smooth acrylic surface as well as transition from floor walking to wall climbing. This robot is intended for inspection and surveillance applications, and ultimately, for space missions.**

***Index Terms*—Dry adhesives, mechatronics, miniature robotics, mobile robotics, wall climbing.**

I. Introduction

MOBILE robots with the ability to climb and navigate on surfaces of any orientation without leaving residue or damaging the surface have many potential applications. One notable situation where such a robot could be useful, and perhaps life-saving, is for spacecraft hull inspection and repair. Terrestrial uses include surveillance or inspection in hazardous or difficult-to-reach areas.

Researchers have proposed a great variety of climbing robots for various applications. Many of the first wall-scaling robots were intended for cleaning in hazardous environments such as nuclear reactors [1]. In general, climbing robots use one of three types of attachment mechanisms: vacuum suction [1]–[7], magnetic attraction [8], or gripping with claws or grasping mechanism [9], [10]. Each of these mechanisms has advantages and drawbacks. For instance, magnetic adhesion can be very strong with the possibility of safe power failure mitigation, but is only applicable for ferromagnetic surfaces. Suction adhesion relies on a complete seal with the surface, making cracked or nonsmooth surfaces problematic, and power efficiency limits their untethered climbing duration. Recently, robots using microclaws have demonstrated climbing capabilities on surfaces such as brick and stone [9], but clawed and grasping robots cannot climb smooth surfaces such as glass or painted structures. To avoid these drawbacks, the robot presented in this paper is designed to ultimately utilize a different type of adhesion mechanism, found in biology, called dry adhesion.

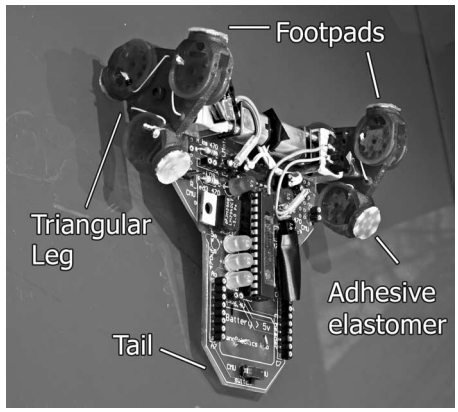

Fig. 1. Photograph of prototype Waalbot climbing a vertical acrylic surface.

This paper presents Waalbot (Fig. 1), a semiautonomous small-scale robot theoretically capable of navigating on smooth flat surfaces of any orientation using adhesive elastomer for attachment. The robot is actuated by two motors, each controlling a three-footed wheel. Unlike many previous implementations of wheel-leg designs such as the ground walking RHex [11], Whegs [12], and miniWhegs [13] robots, Waalbot's legs are specialized for climbing. A miniWhegs climbing robot has been developed, which is able to climb and transition reliably using adhesive tape at high speed (5.8 cm/s), but can only steer very gradually [14]. In contrast, Waalbot climbs with a similar high speed (6 cm/s) but is also able to make sharp turns using a pressure-sensitive dry adhesive elastomer in the place of adhesive tape.

In this paper, Section II describes the adhesive material used for attachment. A static analysis of the forces on the robot is used for optimization of the mechanical design of the attachment mechanism and other robot dimensions in Section III. Also, in Section III, the elastomer adhesion requirements are quantified, and an elastomer is characterized for performance. Robot agility is detailed in Section IV. Experiments on a prototype Waalbot, and its capabilities and performance are described in Section V. Finally, conclusions and future directions are reported in Section VI.

II. Attachment Mechanism

The Gecko lizard's ability to climb surfaces, whether smooth or rough, has attracted scientists' attention for centuries.

Manuscript received March 1, 2006; revised December 15, 2006. Recommended by Guest Editors H.-P. Huang and F.-T. Cheng.

M. Murphy is with the NanoRobotics Laboratory, Department of Mechanical Engineering, Carnegie Mellon University, Pittsburgh, PA 15213-3890 USA. (e-mail: MikeMurphy@cmu.edu).

M. Sitti is with the NanoRobotics Laboratory, Department of Mechanical Engineering, Carnegie Mellon University, Pittsburgh, PA 15213-3890 USA, and also with the Robotics Institute, Carnegie Mellon University, Pittsburgh, PA 15213-3890 USA (e-mail: sitti@cmu.edu).

Digital Object Identifier 10.1109/TMECH.2007.897277

By means of compliant micro/nanoscale high-aspect-ratio beta-keratin structures on their feet, geckos and spiders manage to adhere to almost any surface with a controlled contact area [15]. It has been shown that adhesion is mainly due to molecular forces such as van der Waals forces [16] (from which Waalbot draws its name). Tiny fibers on the animals' feet form weak attractive bonds with the surface, and the combination of billions of contacting fibers creates a large adhesion (up to 100 kPa). Since dry adhesion does not rely heavily on the surface material or atmospheric pressure, it allows climbing on a wide variety of surfaces, and is uniquely suitable for use in the vacuum of space.

Synthetic fibrillar dry adhesive technology is not currently mature enough to be used for climbing robots, however, Waalbot is designed with the intention of eventually utilizing this technology. While efforts to develop the synthetic fibrillar dry adhesive continue [17]–[21], the robot uses polymer adhesive material (Smooth-On Vytaflex 10), which shares many performance characteristics with the envisioned dry adhesive material. Both the dry adhesive and the elastomer adhesive must be pressed to the surface with a preload force in order to provide an adhesive force on detachment. Like fiber-based biological adhesives, compliant elastomers gain their adhesion performance by deforming into the microscale surface features of any smooth surface and creating a large contact area. V10 is highly compliant with a Shore-A hardness rating of 10, and exhibits tack while leaving no residue. Using these adhesives as substitutes until the fiber-based dry adhesives have suitable performance for this application allows testing and improvements to the robot design. The adhesive elastomer is characterized for its adhesion through testing on a custom system. A sample is moved into contact with a substrate that is connected to a high-resolution load cell by an automated stage. When the pressing force reaches a specified preloading value the sample is retracted. The adhesive force is recorded as the maximum force before separation, and force values are converted to pressures by dividing the area of the sample. Fig. 2(a) is a force versus time plot showing the preload (point P_1) and maximum adhesion value (point P_2) from a single experiment. A series of these experiments are performed by varying the preload value and a plot of the adhesion results form a performance curve for the adhesive–substrate combination as shown in Fig. 2(b). This performance curve is typical for the adhesive elastomer tested. The adhesion is greater than the preload pressure for low preload pressures. For higher preload pressures the performance curve saturates at a maximum adhesion value.

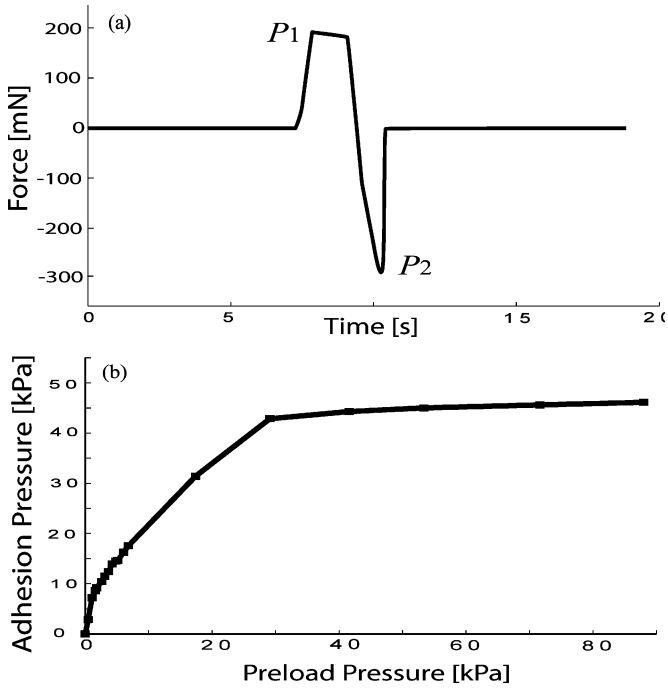

Fig. 2. (a) Typical force versus time data plot for a single adhesion test where P_1 corresponds to the preload and P_2 corresponds to the adhesion. (b) Performance curve for a flat V10 elastomer on a smooth acrylic surface.

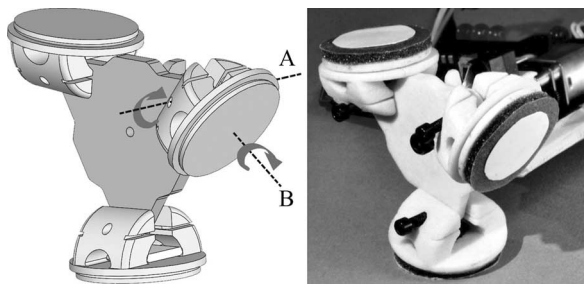

Fig. 3. CAD model of the Tri-Foot design (left) and a photograph of the assembled prototype components (right). Each foot pad has two degrees of freedom enabling climbing and steering. Axis A allows the foot to rotate to maintain contact with the surface. Axis B allows for footpad rotation.

III. Robot Design

A. Mechanical Design

Waalbot's overall mechanical design is discussed in previous work [20]; this section describes the selection of physical parameters for improved performance over initial prototypes.

In order to create a preload force sufficient to bring the adhesive into intimate contact with the surface, a robot should be designed to maximize the pressing force when the adhesive pads come into contact with the climbing surface. This requirement guides the design of the legs and feet. A gear motor's output shaft is connected to a triangular shaped leg (Fig. 3), where each point of the triangle holds a foot assembly on a revolute ankle joint (A). The ankle joint assembly is spring loaded to always return to the forward position (the robot cannot travel in reverse).

On the distal end of the foot assembly is a passive revolute joint (B) connecting a foot pad, which holds the adhesive material. This distal joint enables steering capabilities (discussed later in Section IV). The principle of operation is as follows. During forward travel the two legs are synchronized and step in unison. As the motors turn, the tail of the robot presses against the surface, and the triangular legs rotate forward. The two feet adhered to the surface (one on each side) support the weight of the robot [Fig. 4(a)]. Soon after, the forward feet come into contact with the surface [Fig. 4(b)]. At this point there are five contact points with the surface: two feet on each side and the tail. The motor torque provides an internal moment, which presses the front feet onto the surface while pulling the rear feet away from the surface. When the rear foot normal force F_{Rn} reaches

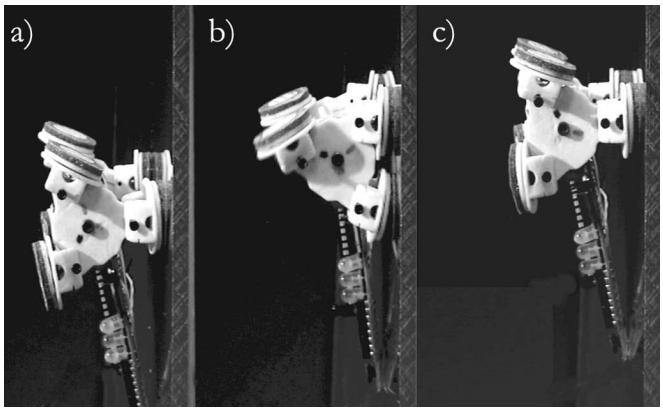

Fig. 4. Still-photograph frames of Waalbot climbing a vertical surface.

TABLE I
PHYSICAL PARAMETERS FOR THE ROBOT MODEL

W	0.69 N
d_{step}	2.6 cm
L_t	6.5 cm
L_{yc}	1.59 cm
L_{xcg}	2.69 cm
L_{yc}	1.49 cm
F_{cr}	0.9 N

a critical peeling value of F_{cr}, the adhesive peels away from the surface and the robot steps forward.

1) Preload-To-Peeling Ratio Analysis: Examining the free body diagram [Fig. 5(a)] and assuming quasi-static dynamics and symmetric loading, it is possible to find a system of equations that describe the forces on the robot during the stepping transfer, represented as

$$\sum F_y = 0 = F_t + F_{Rn} + F_{Fn} - W\cos\theta$$

$$\sum F_x = 0 = F_{Rx} + F_{Fx} - W\sin\theta$$

$$\sum M_c = 0 = (F_{Rn} - F_{Fn})(\frac{d_{\text{step}}}{2}) + F_t(L_t) + W\sin\theta(L_{yc} - L_{ycg}) - (F_{Rx} + F_{Fx})(L_{yc}) - W\cos\theta(L_{xcg}) \quad (1)$$

where W is the weight; θ is the slope of the climbing surface; F_t, F_{Rn}, F_{Fn} are the normal forces at the tail, rear foot, and front foot, respectively. F_{Rx} and F_{Fx} are the shear forces on the rear and front feet, respectively. d_{step} is the distance between the centers of the rear and front feet, L_{yc} is the distance from the climbing surface to the center of the leg, and L_{ycg}, L_{xcg} are the distances from the center of gravity (C_g) to the surface and center of the leg, respectively. L_t is the distance between the center of the leg and the tail–surface contact point. There are five unknown forces ($F_{Fn}, F_{Rn}, F_{Fx}, F_{Rx}$, and F_t) and only three equations, therefore, to solve for the unknowns two assumptions must be made. Assuming $F_{Rn} = -F_{cr}$ will give the forces just before the peel-off occurs, which is when F_{Fn} is at a maximum. We also assume that the shear forces on the front and rear feet are equal ($F_{Fx} = F_{Rx}$). Physical parameters for the model are given in Table 1.

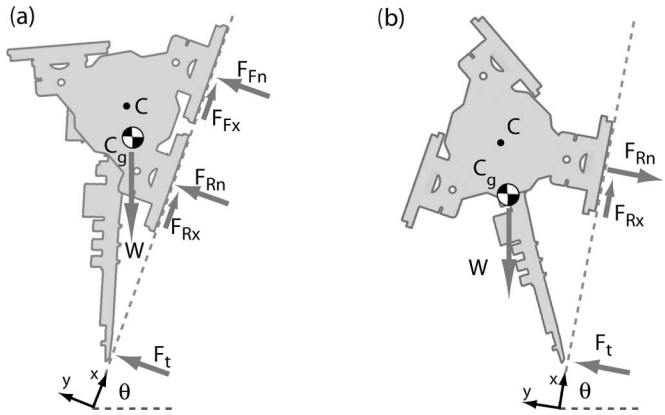

Fig. 5. Free body diagrams showing the forces during a forward step (a) where the front foot is pressed against the surface and the rear foot is peeled, and (b) in the configuration in which the robot experiences the highest peeling force while climbing.

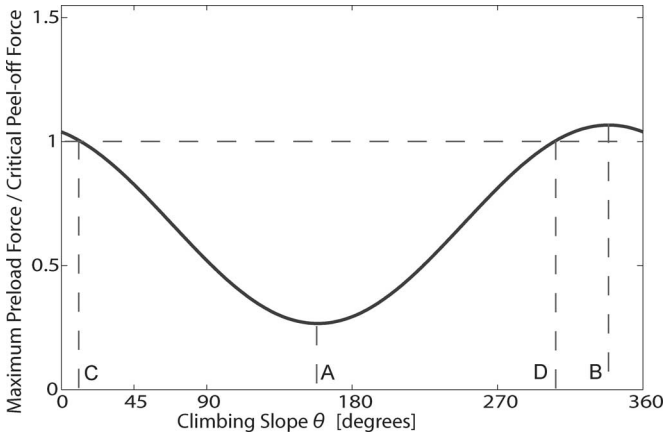

Fig. 6. Plot of preload-to-peeling force ratio for all values of surface slope angle θ with a minimum at 160° (**A**), a maximum at 340° (**B**), and a 1:1 ratio at 11° and 306° (**C**, **D**).

Using these values, assumptions, and (1), it is possible to examine the effect of slope angle θ on the preload force F_{Fn}. Since this preload force presses the adhesive into intimate contact and enables adhesion, it is of critical importance. Specifically, the ratio between the critical peel-off force F_{cr} and the preload force determines the requirements for the adhesive, which are discussed in Section III-B. Using the Waalbot prototype geometry and specifications, the relationship between this ratio and the slope angle is found (Fig. 6).

The graph indicates that for the prototype Waalbot there is a reduction of this ratio up to 73% depending on the climbing angle, with a minimum of 0.266:1 at 160° (close to inverted climbing), meaning that for sustainable climbing the adhesive must consistently provide four times as much adhesion as the force it was preloaded with. The details of this requirement are described in the following section.

2) Critical Peeling Force Analysis: The adhesives have high shear resistance, therefore, detachment occurs due to the normal force pulling the foot away from the surface. The minimum adhesive normal force required to keep the robot attached to the

wall during climbing can be found by examining the case when only one foot per side is attached and the C_g is at its furthest distance from the surface [(Fig. 5(b)]. The quasi-static equation for this case giving a maximum force that the adhesives must be able to provide is represented as

$$F_{Rn} = \frac{W}{L_t}\left(L_{ycg(\max)}\sin\theta - (L_t - L_{xcg})\cos\theta\right). \quad (2)$$

If this force exceeds the magnitude of F_{cr} then, the robot will detach from the surface. Therefore, this equation gives the minimum adhesive performance needed to climb. Because of the consequences of a fall, a safety factor is used when choosing an adhesive and adhesive foot area. Graphing this function with the known design parameters of the robot, it is possible to find the maximum peeling force over all angles. For the prototype parameters the maximum peeling force occurs at a climbing angle of 160°. The corresponding minimum for the critical peeling force of the adhesive F_{cr} is 0.43 N. This value must be supported by the adhesives for the robot to climb on surfaces of all slope angles, and represents one of the adhesive requirements.

From (2), it is clear that in order to minimize the peeling force on the adhesive pad during climbing, the length of the tail should be increased, and the center of gravity should be moved close to the wall. Also, the weight of the robot should be minimized. This can be accomplished through fabricating the robot from lighter materials or through miniaturization. Miniaturization is advantageous to this robot design because mass is proportional to L^3 while the adhesion is proportional to area, i.e., L^2, where L is the characteristic length. As the robot shrinks in size, the adhesion becomes less than the gravitational force, so we see an increase in the performance of the robot.

Both (1) and (2) suggest that the tail should be long to increase the preload force and to minimize the peeling force. However, it is important to note that the weight of the robot is also increased with the tail length, so there is a coupling between W and L_t. Furthermore, a longer tail increases the amount of room necessary for turning, as the tail may sweep out and contact obstacles causing the robot to lose adhesion and fall. So a longer tail limits the ability to climb in small areas. Therefore, for maximum performance without compromising agility, the tail length is chosen to be the longest length possible while remaining fully within the turning circle (described in Section IV). With these parameters fixed, it is necessary to examine the adhesive to determine whether these requirements can be met.

B. Adhesive Requirements

The values from Figs. 2 and 6 and (2) are used to create a set of requirements for the adhesive. For the Waalbot to have the ability to climb on vertical surfaces of $\theta = 90^\circ$, the operating critical peeling force must be no less than 0.16 N (2) and the adhesive must hold with a minimum of two times as much force as it was preloaded with (Fig. 6) at this operating peeling force. To visualize such a requirement it is convenient to plot an adhesive–substrate performance curve with bounds, which represent the requirements as in Fig. 7. Using this representation

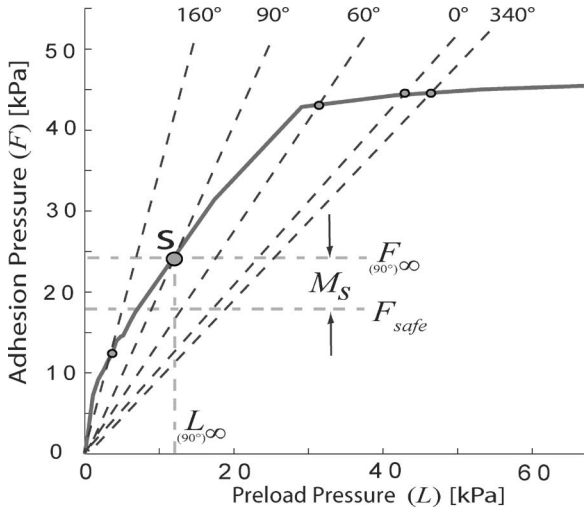

Fig. 7. Performance curve plotted with ratio lines for various surface slope angles. For a surface slope of 90°, the adhesives converge to the steady-state operating preload and adhesion (**s**). L_∞ and F_∞ indicate the steady-state operating preload and adhesion pressure for this slope angle, respectively. F_{safe} indicates a minimum safe adhesion pressure, and the difference between these values is the margin of safety M_s.

it is possible to determine if an adhesive is suitable, and if it is what the minimum footpad size must be.

In Fig. 7, the performance curve is plotted along with lines of various slopes ($m(\theta)$) called "ratio lines" for θ values of $160^\circ, 90^\circ, 60^\circ, 0^\circ$, and 340°. These slopes are the inverse of the ratio of adhesion-to-preload (Fig. 6). The case when the robot is climbing on a surface oriented at 160° was found to be the most challenging [(2), Fig. 6], and appears here as the steepest ratio line while the slope of 340° was found to be the easiest, and has the ratio line with the lowest slope. Ratio lines for all other slope angles fall between these two extremes. In general, the equation of a ratio line is

$$F = m(\theta)L \quad (3)$$

where F is the adhesion pressure, L is the preload pressure, and m is the slope. The performance curve of the adhesive–surface combination [Fig. 2(b)] can be approximated by a power law function (which has similar rising curve and saturation behavior) with general form

$$F = aL^{1/n} \quad (4)$$

where $n > 1$ and a is a scaling coefficient. The preload value at the intersection of the two lines (L^*) is given by

$$L^* = \left(\frac{a}{m}\right)^{\frac{n}{n-1}}. \quad (5)$$

For each step the robot has an initial preload L_i. The maximum peeling pressure F_i is determined by the performance curve. This maximum adhesion pressure is transferred to the preload pressure for the next step with a force ratio of $1/m$. To determine the steady-state operating adhesion and preload (the pressures at which the feet will press onto and adhere to the surface after many steps), we examine an iterative function where each iteration represents one forward step of the robot.

It can be shown that the preload converges to the intersection preload (L^*) through an iterative proof using the update rule

$$L_{i+1} = \left(\frac{a}{m}\right) L_i^{\left(\frac{1}{n}\right)} \tag{6}$$

which mathematically represents a single step, where L_i is the preload for step number i. The steady-state operating preload (L_∞) is given by

$$L_\infty = \lim_{n\to\infty} \left(\frac{a}{m}\right)^A L_0^{\left(\frac{1}{n}\right)} \tag{7}$$

$$A = 1 + \frac{1}{n}\left(1 + \frac{1}{n}\left(1 + \frac{1}{n}(\ldots)\right)\right) = \frac{n}{n-1}. \tag{8}$$

Therefore,

$$L_\infty = \left(\frac{a}{m}\right)^{\frac{n}{n-1}} = L^*. \tag{9}$$

The steady-state operating preload (L_∞) converges to the preload at the intersection of the two lines (L^*) from (5). The steady-state operating adhesion (F_∞) is then equal to mL_∞. These two values define a *steady-state operating point*, point **S** in Fig. 7. There is also a minimum safe adhesion value (F_{safe}), which is a function of the area of the footpads and the surface slope angle θ, and can be calculated from (2) and foot size. The steady state operating adhesion (F_∞) must be greater than the minimum safe adhesion value (F_{safe}) to prevent the robot from detaching from the climbing surface. The margin between the steady-state operating adhesion and the minimum safe adhesion is the margin of safety (M_s). Since the robot will not always have ideal force transfer on every step, it is important to have a large margin of safety so that the robot can recover from a problematic step, or continue to operate if the adhesives become contaminated and function with degraded performance.

It is possible to increase the margin of safety by increasing the area of the adhesives (foot pad size), which lowers the minimum adhesion pressure requirement. However, there is a tradeoff because the motors then need to provide more torque to peel the larger feet. This causes an increased power requirement, which leads to larger batteries, and also necessitates a larger and heavier motor.

C. Robot Fabrication

A printed circuit board (PCB) acts as the chassis for the robot instead of using an additional body frame in order to keep the mass low. The leg and feet assemblies are fabricated via 3-D printing (Z-Corp. ZPrinter and 3-D Systems Invision HR). The heaviest components of the system are the leg assemblies, motors, and batteries. In order to move the center of gravity as close as possible to the surface and balanced around the motor axes, all these parts are located close to the shaft axes with the batteries beneath the PCB, nearly in contact with the climbing surface.

The robot is controlled by a PIC microcontroller (PIC16F737), and is able to perform preprogrammed actions such as climbing and turning without instructions from the user. Gait is controlled with feedback from foot position sensors. Limit switches are triggered when the legs are aligned so that only one foot on each side is in contact with the surface. This information is used to keep the robot's gait synchronized by pausing one of the motors until the opposing motor catches up, assuring that the assumptions of symmetry in (1) are valid. Foot position tracking is also important for safely putting the robot into steering mode. Infrared (IR) RC5 communication is used to teleoperate the robot to climb straight, stop, and turn. Commands can be sent for turning 180°, 90°, and in increments of 15° in either direction.

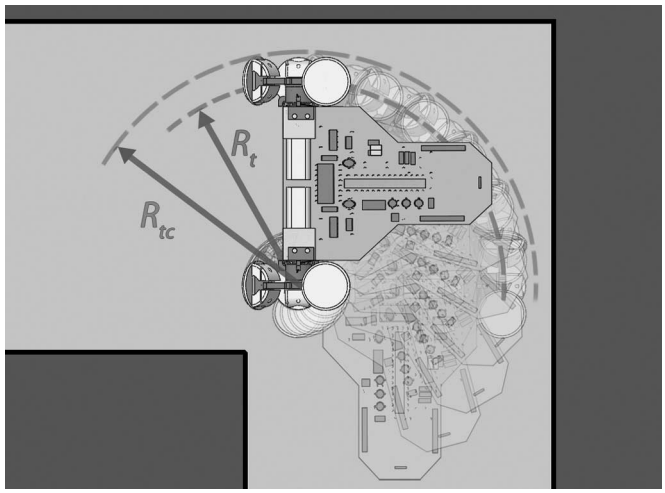

Fig. 8. Waalbot's small turning radius (R_t) and turning circle radius (R_{tc}) allow it to climb around obstacles, and operate in narrow corridors with sharp bends.

Power is provided by two lithium ion polymer batteries which are placed in series beneath the body of the robot for 7.4 V. The two motors (Sanyo 12GA-N4s) have a torque output of approximately 400 mN.m each, which is sufficient to peel the rear feet from the surface.

IV. Agility

A. Steering

When only one foot on a side is in contact with the surface, that foot can be used as a pivot point for the robot to rotate about. By advancing the opposite motor, the robot rotates around the passive revolute joint in the pivoting foot. If the robot attempted to turn while the two feet were attached on a side, the robot would shear itself off the surface, since the center of rotation would not be aligned with a joint. Since this can be a catastrophic failure for a climbing robot, foot position sensors are used to prevent this occurrence.

In steering mode, the robot takes discrete steps around the pivoting foot. The turning radius is less than the width of the robot, which allows tight turns (Fig. 8). The ability to make tight turns is an important feature for climbing through small passageways or for avoiding closely spaced obstacles.

Steering angle per step can be calculated from the turning radius R_t and the stepping distance d_{step} by examining the triangle between the pivot, front, and rear stepping feet as

$$\theta = \cos^{-1}\left(1 - \frac{d_{\text{step}}^2}{2R_t^2}\right) \tag{10}$$

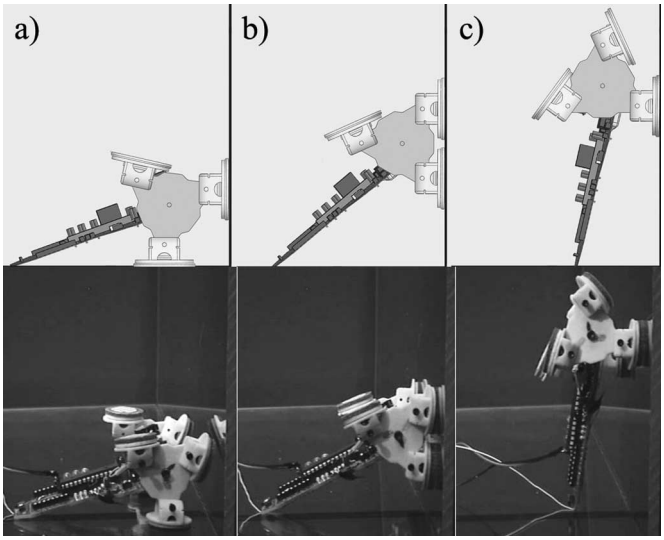

Fig. 9. Schematic side view showing the steps in a 90° plane transition (top) and still-photograph frames of the Waalbot prototype performing the transition (bottom).

where the turning radius R_t is the lateral distance between the centers of the feet. Conversely, given a desired stepping angle, the robot's dimensions can be designed to achieve this angle.

The prototype Waalbot was designed to make discrete turning increments, which change the heading by $15°$/step. This angle is convenient as it allows for turns of $45°, 90°$, and $180°$ as well as smaller adjustments.

B. Plane Transitions

The robot's unique jointed legs allow it to perform transitions between planes. For example, the robot can theoretically climb along a floor and transition to climbing up a vertical wall, and then, transition onto another wall or a ceiling. The steps of a transition process are shown in Fig. 9. As the robot approaches a junction, the forward foot makes contact with the new plane [Fig. 9(a)], and the robot makes the planar transition [Fig. 9(b) and (c)]. The Tri-Foot design gives Waalbot the capability of making planar transitions of various angles including $90°$, however, the transitions are not fully robust. This is due to the nonperpendicular angle at which the forward foot may contact the new plane. Since the foot position is optimized for flat surface walking, when a new plane is encountered the foot may not come into full contact immediately. In this case, the foot may not be preloaded correctly, and adhesion cannot be guaranteed. In the worst case, the forward foot may land in the junction, touching both planes and making very little contact, causing almost certain failure of adhesion. Therefore, depending on the relative angles of the approaching foot and the new plane, the robot may or may not successfully make the transition. However, for any given angle between the two planes down to an acute $60°$, there exists a series of foot placements that will allow for a successful transition. The distance from the final step in the first plane to the junction determines the angle between the approaching foot and the new plane, and the optimal foot placement can be calculated if the angle between the two planes is known. It may be possible to incorporate capabilities to calculate this optimal foot placement when a new plane is detected, and then plan a sequence to transition successfully.

TABLE II
SPECIFICATIONS OF THE ROBOT PROTOTYPE IN EXPERIMENTS

Weight	0.69 N
Length	13 cm
Height	5 cm
Width (total)	12.3 cm
Turning Radius (R_t)	10 cm
Turning Circle Radius (R_{tc})	11.15 cm
Step Length (d_{step})	2.6 cm
Adhesive Area (per foot)	1.1 cm^2

A prototype Waalbot was built according to the design aspects previously mentioned with the specifications given in Table II. The foot pad area was designed according to the adhesive requirements for $90°$ climbing.

V. EXPERIMENTS

A. Force Characterization

A force plate system was created to experimentally confirm the theory in Section III. To measure the forces during climbing, the Waalbot prototype climbs on an acrylic sheet with a small circular acrylic panel. This circular panel is supported by a thin rectangular steel cantilever beam. Using a laser scan micrometer (Keyence LS-3034) to measure the beam deflection, the force on the circular panel can be determined. During operation the force plate moves only a few hundred micrometers, and therefore, approximates a rigid surface. The force plate system can be adjusted to any angle so that testing can be done at all surface slopes.

This test setup allows measurements of normal forces between the robot and the climbing surface such as F_{Rn} and F_{Fn} for comparison with (1) and (2).

To validate the results from (2) the Waalbot prototype was placed on the acrylic sheet with one footpad adhered to the force plate in the configuration from Fig. 5(b). The normal forces were recorded for surface slopes from $0°$ to $180°$ at $30°$ increments and at $300°$. The measurement apparatus was calibrated by taking the measurements without the Waalbot so that the weight effects of the force plate could be removed from the results. The results are plotted against the theoretical results in Fig. 10. The close match between the experimental data and (2) confirms the adhesion requirement model for the direction normal to the surface for the configuration seen in Fig. 5(b).

Using the same force plate system, we can compare the performance curve data from material tests (Fig. 7) to its performance in use on the Waalbot. The prototype is directed to step onto and off the force panel, and the preload and associated pull-off forces are recorded. The robot was tested with a surface slope of $\theta = 0$ for simplicity. The experimental adhesion and preload pressures are found by dividing the preload and pull-off forces by the foot area. Fig. 11 shows the experimental preload pull-off data and material testing performance curves overlayed for comparison. Here, each data point represents a single step as the Waalbot steps onto and off the force plate, and

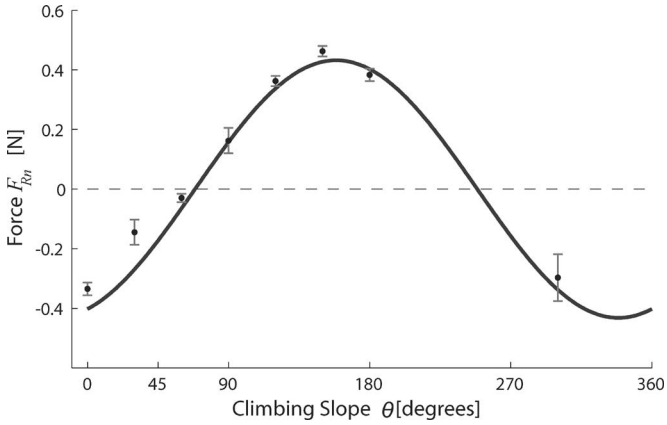

Fig. 10. Experimental normal forces (points) agree with theory (line) from (2) for varying climbing slopes. Error bars indicate the standard deviation of the measured values.

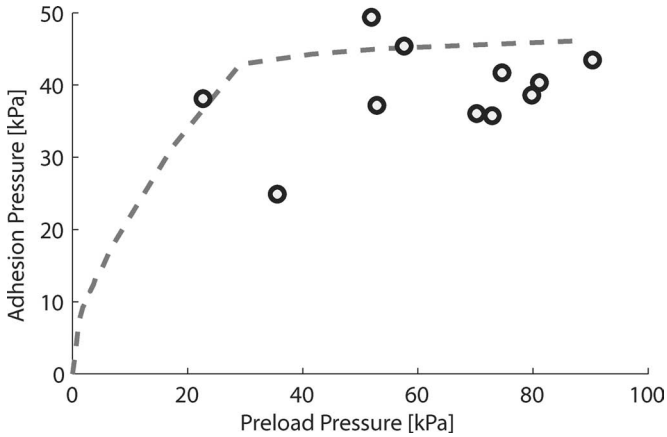

Fig. 11. Data from Waalbot experiments on force plate overlayed on the performance curve from material testing (dotted line).

each point is from a different run. Although the data from the Waalbot prototype experiments do not exactly match the performance curve generated from the material testing, the agreement is sufficient to demonstrate that the material testing performance curve is a reasonable estimate for the real robot performance, and can be a useful tool for selecting an adhesive material and footpad size. Most of the data points show slightly reduced adhesion compared to the performance curve data. However, this is expected since the material testing was carried out in a highly controlled and physically constrained set of experiments, whereas the Waalbot prototype experiments represent a larger scale adhesive behavior. Possible sources for discrepancy include incomplete attachment of the foot pad to the surface, speed of attachment and detachment, and peeling effects due to the spring-loaded ankle joint.

B. Climbing Performance

The current Waalbot prototype was tested on a smooth clear acrylic climbing surface. It is capable of climbing any direction on planes of various orientations. This includes climbing up, down, or across a vertical (90°) surface, all at speeds of up to 6 cm/s, which is limited by the motor speed. The robot climbing speed was measured by examining video of the prototype climbing up a distance of 30 cm. Similarly, the maximum turning speed was found to be approximately 37°/s. The maximum angle, which the prototype is able to climb, was found to be 110° (20° past vertical). The robot is able to remain adhered to an inverted surface, but detaches when stepping. It was observed that the footpads peel off from the surface at the leading edge, indicating that the assumption in our analytical model of a point force at the center of the foot is not valid, since there is a nonuniform load across the adhesive surface.

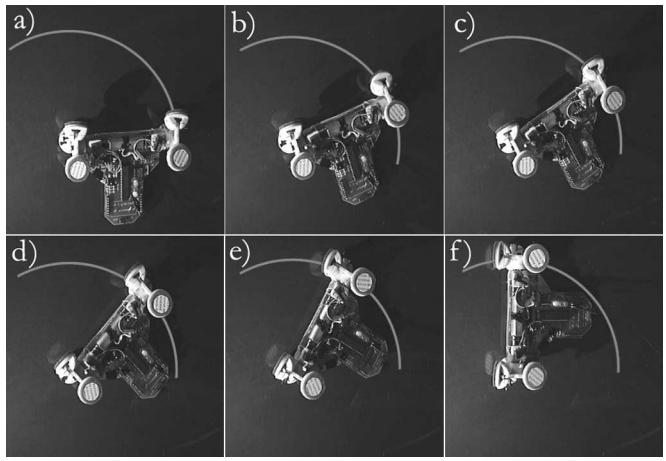

Fig. 12. Still frames from a video showing a Waalbot prototype turning while climbing on a vertical acrylic surface. The prototype turns 90° (line overlayed) in six steps (a)–(f).

The prototype Waalbot is able to make left- and right-hand turns without falling from the climbing surface (Fig. 12). Both small and large turning angles are routinely made. The prototype can be teleoperated to navigate around obstacles while climbing.

The current prototype is capable of making transitions of various angles, including 90°. Floor to wall, and wall to floor transitions were successfully accomplished. Ceiling to wall and wall to ceiling transitions were not successful. As discussed in Section IV-B, the transitions are not robust; the prototype feet often land in the corner causing the robot to lose adhesion with the climbing surface. Videos of the prototype performing various agility tasks can be viewed at http://nanolab.me.cmu.edu/projects/waalbots/tri-leg.html.

VI. Conclusion

A wall-climbing robot design was analyzed and implemented. A quasi-static model was created to determine the forces acting on the robot. A model for adhesive performance for a climbing robot was developed, which demonstrates the margin of safety and steady-state operating points. Design criteria were established to guide adhesive selection, foot size, and torque requirements. A semiautonomous tetherless robot prototype was designed and fabricated, which is able to climb on smooth surfaces of various orientations including climbing in any direction on smooth vertical acrylic surfaces using a pressure sensitive elastomer for attachment. The robot can climb at a speed of 6 cm/s (0.46 body length/s), and turn with a small turning radius

to travel along curved paths and around tight corners. IR communication is used to control the robot. The prototype was not able to climb on inverted surfaces because of its high mass, but was able to climb on smooth acrylic surfaces with slopes up to 110° and make floor to wall transitions.

Climbing reliability of the prototype was limited because of the inability of the robot to maintain synchronization between the two legs. The sensors synchronize the legs only three times per revolution. Since the motors and drive trains differ slightly in friction, they run at different speeds. While the sensors are sufficient for foot positioning for safe turning, they do not provide synchrony throughout forward steps. When the feet are stepping even slightly asynchronously the assumptions made for the robot analysis no longer apply. In this case, the front feet are not necessarily preloaded correctly and the robot often falls. Future versions of the Waalbot will utilize absolute encoders to track and synchronize the legs.

One of the major disadvantages of this robot design is that there is very little redundancy in case of adhesion failure. Most of the time, there are only two feet attached to the surface. Inverted climbing was not possible with the prototype due to the mass of the robot. As the adhesives used on the feet of the robot gathered dust and other contaminants, their performance degraded quickly. Therefore, these elastomer adhesives are not suitable for dirty outdoor environments, walking across indoor floors, or for long term tasks. Furthermore, if improper foot placement occurs, the possibility of adhesion failure during a plane transition is a dangerous flaw for a climbing robot. Sensing and planning for plane transitions is an important future challenge.

Future work includes implementing the synthetic dry adhesives in place of the conventional adhesives when the technology is mature. Further miniaturization of the robots is required to improve performance due to increased area-to-mass ratio. Decreasing the robot mass will increase payload capacity, allowing for other sensors or tools, and lower power consumption for longer operation time. The force model will be improved by including the ankle joint as well as nonuniform adhesion pressure distribution across the surface of the footpads. Initial results from tests with a new smaller scale prototype, which addresses many of the issues discussed, show that these challenges can be overcome and suggest that reliable climbing with this design is possible.

ACKNOWLEDGMENT

The authors would like to thank W. Tso and M. Tanzini for their robot design, fabrication, and testing assistance, and all the members of the NanoRobotics Laboratory at Carnegie Mellon University for their help and discussions.

REFERENCES

[1] W. Yan, L. Shuliang, X. Dianguo, Z. Yanzheng, S. Hao, and G. Xueshan, "Development and application of wall-climbing robots," in *Proc. IEEE Int. Conf. Robot. Autom.*, 1999, pp. 1207–1212.

[2] S. Hirose, A. Nagakubo, and R. Toyama, "Machine that can walk and climb on floors, walls and ceilings," in *Proc. Int. Conf. Adv. Robot.*, 1991, vol. 1, pp. 753–758.

[3] S. Ryu, J. Park, S. Ryew, and H. Choi, "Self-contained wall-climbing robot with closed link mechanism," in *Proc. Int. Conf. Intell. Robots Syst.*, 2001, vol. 2, pp. 839–844.

[4] L. Briones, P. Bustamante, and M. Serna, "Wall-climbing robot for inspection in nuclear power plants," in *Proc. Int. Conf. Robot. Autom.*, 1994, pp. 1409–1414.

[5] R. Pack, J. L. Christopher, and K. Kawamura, "A rubbertuator-based structure-climbing inspection robot," in *Proc. IEEE Int. Conf. Robot. Autom.*, Albuquerque, NM, 1997, vol. 3, pp. 1869–1874.

[6] B. Luk, A. Collie, V. Piefort, and G. Virk, "Robug iii: A tele-operated climbing and walking robot," in *Proc. UKACC Int. Conf. Control*, 1996, vol. 1, pp. 347–352.

[7] T. Yano, T. Suwa, M. Murakami, and T. Yamamoto, "Development of a semi self-contained wall climbing robot with scanning type suction cups," in *Proc. Int. Conf. Intell. Robots Syst.*, 1997, vol. 2, pp. 900–905.

[8] J. Grieco, M. Prieto, M. Armada, and P. Gonzalez de Santos, "A six-legged climbing robot for high payloads," in *Proc. Int. Conf. Control Appl.*, 1998, pp. 446–450.

[9] S. Kim, A. T. Asbeck, M. R. Cutkosky, and W. R. Provancher, "Spinybot II: Climbing hard walls with compliant microspines," in *Proc. Int. Conf. Adv. Robot.*, 2005, pp. 601–606.

[10] T. Bretl, S. Rock, and J.-C. Latombe, "Motion planning for a three-limbed climbing robot in vertical natural terrain," in *Proc. Int. Conf. Robot. Autom.*, 2003, pp. 2947–2953.

[11] R. Altendorfer, N. Moore, H. Komsuoglu, M. Buehler, H. B. B. Jr., D. McMordie, U. Saranli, R. Full, and D. Koditschek, "Rhex: A biologically inspired hexapod runner," *Auton. Robots*, vol. 11, no. 3, pp. 207–213, 2001.

[12] R. Quinn, D. Kingsley, J. Offi, and R. Ritzmann, "Improved mobility through abstracted biological principles," in *Proc. IEEE/RSJ Int. Conf. Intell. Robots Syst.*, 2002, pp. 2652–2657.

[13] J. M. Morrey, B. Lambrecht, A. D. Horchler, R. E. Ritzmann, and R. D. Quinn, "Highly mobile and robust small quadruped robots," in *Proc. Int. Conf. Intell. Robots Syst.*, 2003, vol. 1, pp. 82–87.

[14] K. Daltorio, A. D. Horchler, S. Gorb, R. Ritzmann, and R. Quinn, "A small wall-walking robot with compliant, adhesive feet," in *Proc. Int. Conf. Intell. Robots Syst.*, 2005, pp. 4018–4023.

[15] K. Autumn, Y. A. Liang, S. T. Hsieh, W. Zesch, W. P. Chan, T. W. Kenny, R. Fearing, and R. J. Full, "Adhesive force of a single gecko foot-hair," *Nature*, vol. 405, pp. 681–685, 2000.

[16] K. Autumn, M. Sitti, Y. A. Liang, A. M. Peattie, W. R. Hansen, S. Sponberg, T. W. Kenny, R. Fearing, J. N. Israelachvili, and R. J. Full, "Evidence for van der waals adhesion in gecko setae," *Proc. Nat. Academy Sci.*, vol. 99, pp. 12 252–12 256, 2002.

[17] M. Sitti and R. Fearing, "Synthetic gecko foot-hair micro/nanostructures as dry adhesives," *J. Adhesion Sci. Technol.*, vol. 17, no. 5, pp. 1055–74, May 2003.

[18] A. K. Geim, S. V. Dubonos, I. V. Grigorieva, K. S. Novoselov, A. A. Zhukov, and S. Y. Shapoval, "Microfabricated adhesive mimicking gecko foot-hair," *Nature Mater.*, vol. 2, pp. 461–463, Jun. 1, 2003.

[19] N. J. Glassmaker, A. Jagota, C.-Y. Hui, and J. Kim, "Design of biomimetic fibrillar interfaces: 1. making contact," *J. R. Soc., Interface*, vol. 1, no. 1, pp. 23–33, Nov. 2004.

[20] C. Menon, M. Murphy, and M. Sitti, "Gecko inspired surface climbing robots," in *Proc. IEEE Int. Conf. Robot. Biomimetics*, 2004, pp. 431–436.

[21] B. Aksak, M. Murphy, and M. Sitti, "Adhesion of biologically inspired vertical and angled polymer microfiber arrays," *Langmuir*, vol. 23, no. 6, pp. 3322–3332, 2007.

Michael P. Murphy (M'07) received the B.Sc. degree in mechanical engineering from Yale University, New Haven, CT, in 2003, and the M.Sc. degree in mechanical engineering from Carnegie Mellon University, Pittsburgh, PA, in 2005, where he is currently working toward the Ph.D. degree.

His current research interests include mobile robot systems, biologically inspired miniature robots, and micro/nanoscale smart materials.

Mr. Murphy received the Best Biomimetics Paper Award at the 2004 IEEE International Conference on Robotics and Biomimetics.

Metin Sitti (S'94-M'00) received the B.Sc. and M.Sc. degrees in electrical and electronic engineering from Bogazici University, Istanbul, Turkey, in 1992 and 1994, respectively, and the Ph.D. degree in electrical engineering from the University of Tokyo, Tokyo, Japan, in 1999.

He was a Research Engineer in the Computer-Aided Design/Computer-Aided Manufacturing (CAD/CAM) Robotics Department, TUBITAK Marmara Research Center, Kocaeli, Turkey, during 1994–1996. He was a Research Scientist and a Lecturer in the Department of Electrical Engineering and Computer Sciences, University of California, Berkeley, during 1999–2002. He is currently an Assistant Professor in the Mechanical Engineering Department, Carnegie Mellon University (CMU), Pittsburgh, PA, and the Robotics Institute, CMU. His current research interests include micro/nanoscale robotic dynamics, systems, and control, biologically inspired miniature robots, and micro/nanoscale manipulation and manufacturing systems.

Dr. Sitti received a National Science Foundation CAREER Award and the CMU Struminger Award in 2005. He was elected a Distinguished Lecturer for the IEEE Robotics and Automation Society for 2006–2008. He received the Best Paper Award at the IEEE/RSJ International Conference on Intelligent Robots and Systems in 1998, the Best Video Award at the IEEE Robotics and Automation Conference in 2002, and the Best Biomimetics Paper Award at the IEEE Robotics and Biomimetics Conference in 2004.